Real-Time Pressure Estimation and Localisation with Optical Tomography-inspired Soft Skin Sensors

Abu Bakar Dawood[1], Brice Denoun[2], and Kaspar Althoefer[1]

***Abstract*— Sensing and localising pressure resulting from physical interaction between a robot and its environment is a key requirement in the deployment of soft robots in real-life scenarios. In order to adapt the robot's behaviour in real-time, we argue that sensors must have a high sampling rate. In this paper, we present a novel tactile sensing strategy for soft sensors, based on an imaging technique known as optical tomography. Instead of transmitting light through the soft sensor in a sequential way (as commonly done in tomography systems), we demonstrate that concurrently illuminating the sensor with multiple light sources and reading out the sensor response has several advantages. Firstly, it drastically increases the sampling rate of the sensor when compared to standard tomography approaches, making it more suitable to sense sudden and short-lived contacts. Secondly, by concurrently switching on the light sources, we increase performance in terms of pressure localisation and pressure estimation achieved through Machine Learning techniques. We carry out experiments demonstrating that our approach allows for a robust pressure estimation and contact point localisation with an accuracy up to 91.1% (vs 70.3%) at a higher sampling rate.**

I. Introduction

Interest in soft robotics from the scientific community has dramatically increased over the last decade [1]. This is especially true for use-cases in which the lack of compliance of traditional robots creates issues, such as in human-robot interaction scenarios [2]. Indeed inherent compliance is the fundamental characteristic of soft robots that renders them ideal candidates for use in close proximity to humans - a consequence of the minimal risk they pose of inflicting damage on their immediate environment [3], [4].

A key attribute of soft robots is their infinite degree of freedom. This however creates challenges in terms of accurately modelling their kinematics or accurately controlling their soft bodies [5]. For this reason, making soft robots capable of proprioception (i.e. having a sense of its movement and position) and exteroception (i.e. having a sense of external stimuli) would provide them with crucial information about their own state [6] as well as the way in which they interact with the environment [7]. However, proprioception and exteroception in soft robots cannot be achieved using traditional rigid sensors because their lack of compliance would compromise the advantageous degrees of freedom offered by the robots' soft bodies. For this reason, a wide range of soft sensors have been proposed in the literature [8], that can be integrated into soft robots [9]. These sensors make use of a variety of sensing modalities, such as resistive [7], capacitive [10], magnetic [11] or optical [12] modalities.

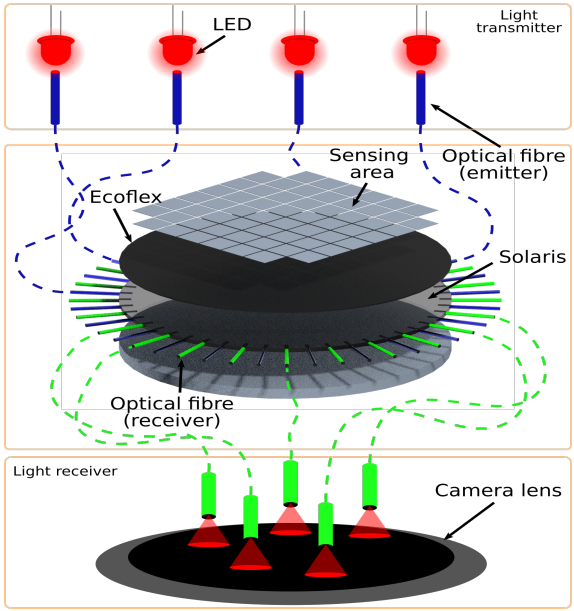

Fig. 1: Soft sensor skin based on optical tomography using optical fibres as a mean to emit and receive light. The skin can easily be applied on any surface and only contains soft and deformable components, without any embedded electronics.

In this work, we investigate a novel tactile sensing strategy for optical tomography inspired soft skin sensors and show the skin's ability to localise and estimate the pressure applied to it using Machine Learning (ML) techniques. We show that using multiple sources of light to illuminate the skin concurrently not only increases the sampling rate but also improves the performance of pressure estimation and localisation.

II. Related Works

As previously mentioned, exteroceptive soft sensors must be compliant, so that they do not compromise the deformable structure and movement of soft robots. One of the most direct applications of exteroception is to estimate where and how much pressure is applied to the body of a soft robot, as it can

*Work supported by a research grant from the Engineering and Physical Sciences Research Council (EPSRC), in the framework of the National Centre for Nuclear Robotics (NCNR) project (EP/R02572X/1). We also thank Hareesh Godaba and Faisal Aljaber for their input in this research.

[1]Abu Bakar Dawood and Kaspar Althoefer are with the School of Engineering and Materials Science, Queen Mary University of London, London E1 4NS, UK a.dawood@qmul.ac.uk

[2]Brice Denoun is with the School of Electronics Engineering and Computer Science, Queen Mary University of London, London E1 4NS, UK

provide valuable information about its collision state with the environment [13]. Previously employed methodologies based on micro-fluidic [14], resistive [7], Electric Impedance Tomography (EIT) [**?**], magnetic [11] or capacitive [15] sensing modalities have been integrated into soft artificial skins [16]. These skins are generally composed of arrays of sensors exploiting either one [10] or several sensing modalities [17]. Although such works demonstrate promising results, producing these sensors can be expensive and time consuming. In addition, these sensing technologies are susceptible to environmental noise. By way of example, the input and output values of magnetic and capacitance-based sensors are highly dependent on whether they are located in ambient magnetic fields, possibly generated by a nearby computer or robot.

Soft optical force and tactile sensors have become more popular for a host of reasons, including low cost, isolation from electromagnetic noise and due to advancements in data-driven approaches, such as image processing and Machine Learning. For instance, GelSight [18], TacLINK [19] and F-Touch [20] sensors have demonstrated a striking breakthrough in light based force sensing and high resolution feature estimation. These sensors work on the reflection of light from an elastomer having different patterns; as the camera underneath the elastomer detects the changes, it can estimate force, direction and geometry of the object placed on top of it. However, the position of the camera with respect to these patterns greatly impacts the sensing performance, restricting their use in exteroceptive sensing in deformable soft robots.

More recently, Amoateng et al. have proposed an optical tomography-based soft skin capable of estimating the localisation and amount of force applied by external contacts [21]. The fabrication process of this skin-shaped sensor is simpler than that of camera-based sensor systems as it consists of an optically transparent PDMS layer surrounded by infrared (IR) emitters and receivers on a flexible circuit. However, the proposed design suffers from two main shortcomings. Firstly, the optically transparent layer is not well isolated from ambient light, meaning that any changes in the lighting conditions will greatly impact both the input and output of this sensor. Secondly, their 24 IR emitters are switched on and off sequentially (i.e. each IR receivers will record 24 values; one for each emitter), resulting in a low sampling rate of the sensor.

To overcome these limitations, we propose a novel strategy to acquire data from optical tomography based soft skin sensors that allows us to obtain real-time pressure estimation and localisation. We demonstrate the advantages of our approach on a light-isolated soft skin sensor that uses 48 optical fibres (24 of which emit light and the remaining 24 of which receive light) instead of IR receivers/emitters to remove any rigid or electronic components from the sensing area (see Figure 1). A set of experiments presented in section IV show that the proposed data collection methodology increases the sensing capabilities of optical tomography based soft sensors.

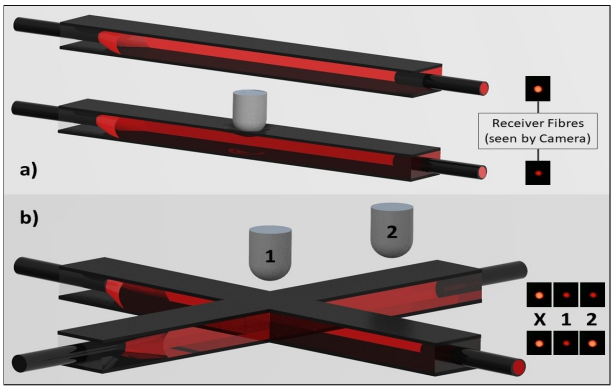

Fig. 2: Light as seen by the camera through the transparent silicone. a) shows the light intensity at the end of receiver fibre with and without indentation. The reduction in light intensity is proportional to the indentation. b) shows two transparent silicone layers perpendicular to each other. X shows the intensity of light from optical fibres when there is not indentation. 1 shows the intensity when indenter 1 is used. 2 shows the intensity of both the fibres when indenter 2 is used.

III. Optical sensorised skin

A. Principle

Optical tomography is a technique that is extensively used in non-invasive medical imagery [22]. By analysing light transmitted and scattered through an object, such as soft tissue in a medical diagnostic scenario, this technique allows us to estimate a range of object properties such as its geometry and structure. With soft transparent materials, optical tomography can be applied to estimate the pressure that caused the deformation of the material.

Figure 2a shows the change in light intensity observed by an optical fibre when a transparent silicone layer is mechanically indented. When multiple light sources intersect, the data captured by the receivers contains crucial information about where the force has been applied. This is illustrated with two pairs of optical fibres in Figure 2b, where the intensity of light received by the two receivers changes depending on the location of the indentation. In fact, when a local force is applied (e.g. by an indenter) at the intersection of two light rays, the intensity captured by both the receivers will decrease. On the other hand, if a local force is applied at a location covered by only one pair of optical fibres, the other receiver will not detect any change in the captured light.

Based on this principle, we have designed a circular skin with 24 emitter and 24 receiver optical fibres alternately distributed around the circumference of a soft transparent silicone skin (see Figure 4). Further details about the design of the skin are discussed in the next subsection.

B. Design

The design of the skin used in this work is similar to the one proposed in [21]; 24 emitters and 24 receivers are encapsulated in a soft transparent layer that can be applied onto any surface. However, instead of using 2mm thick

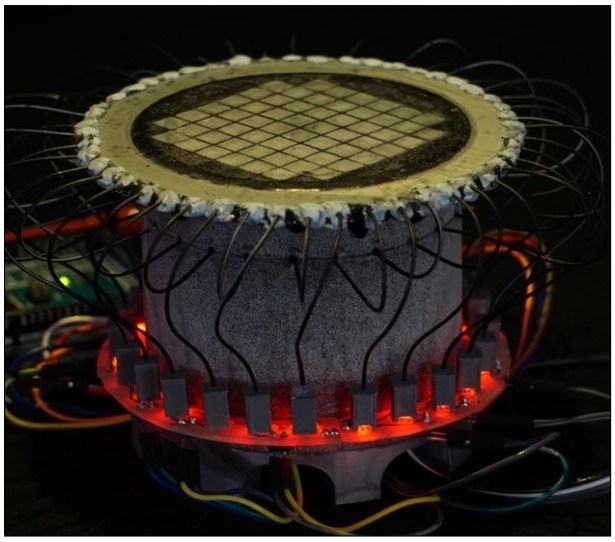

Fig. 3: The experimental setup. Figure shows the optical skin on a 3D printed tray holding the optical fibres. The tray is fixed on a 3D printed hollow cylinder that acts as camera housing and PCB holder for the LEDs.

PDMS for the optical layer, we opt for a more compliant 1.2mm thick Solaris Smooth-On layer (Shore Hardness 15A). We propose to use 1mm-diameter optical fibres (Mitsubishi ESKA FF-SH 2001-J) to transmit and receive red light (with a wavelength of 633nm). The use of optical fibres enables us to remove any electronics from the sensing element, making it more suitable for the remote deployment of soft robots (see Figure 1). To isolate the transparent Solaris layer from ambient light, a soft 0.2mm thick black EcoFlex layer (shore 00 hardness of 30) is added on top of it. This layer also protects the Solaris layer from damage during physical interaction with the environment.

The total diameter of our skin is 80mm, with optical fibres embedded 7.5mm into the transparent layer, leaving an effective sensing area of 65mm in diameter. We discretize this area into 60 sectors by brushing aluminium powder on top of the protective black EcoFlex layer. Each sector has an area of 56.25mm^2 ($7.5\text{mm} \times 7.5\text{mm}$) allowing us to test the spatial resolution of our skin down to 7.5mm increments.

In this experiment, the optical skin was put in a 3D printed dish with the skin and the twenty-four emitter and receiver pairs of optical fibres firmly held in place. This supporting dish was then placed on top of a hollow cylinder that also supports the 24 LEDs, acting as source of light. We designed a circular Printed Circuit Board (PCB) to mount the LEDs. To minimise light loss due to scattering and refraction, we used higher wavelengths of the visible spectrum; i.e. we used LEDs (LS E63B-BBCB-1-1) emitting light at a wavelength of 633nm. 3D-printed opaque casings were used to cover the LEDs and hold the emitting fibres in front of the LEDs (see Figure 3). The tips of the optical fibres were sanded and polished to minimise light losses during transmission from the LEDs to the Solaris layer. Figure 4 shows the illuminated skin without the top protective black EcoFlex layer. As highlighted in this figure, each emitter fibre emits light in a conical form and illuminates three to four receiver fibres on the opposite side of the skin.

All the LEDs are connected to a Raspberry Pi 3B+, which allows us to individually control each LED. This way, with the same connections, we are able to carry out sequential and concurrent LED switching, to compare these two types of tomography methods. Each receiver optical fibre is also cut to size, sanded and polished to minimise losses and one end is embedded into the transparent layer. The other end of each receiver optical fibre is isolated from ambient light and fixed in front of the camera, set in a 3D printed casing housed inside the hollow cylinder. Rather than using individual photo-sensors, we preferred a commercially available RGB camera to estimate the light intensity of each optical fibre as it is both cheaper and more compact. The camera we chose is a Logitech C310 webcam which captures images with a resolution of 1280x720 pixels at a rate of 30 frames per second. The focus of the camera was manually adjusted to ensure that the output of each optical fibre produces a well-focused image. It is important to note that using a more high-end camera would allow the sensor to capture data up to 120Hz.

C. Sensor reading

In [21], the authors propose sequentially transmitting light through a PDMS layer, i.e. the 24 emitters are sequentially switched on and off. The signal sent by each emitter lasts 2.5 ms and results in 24 values read by the integrated photodetectors. Therefore, a full reading of the skin is represented by 576 values collected over at least 60 ms, corresponding to a final sampling rate of at most 15Hz. This approach has been shown to be efficient in estimating and locating pressure on a soft optical-based sensorised skin. Figure 5b shows a subset of two images captured by our camera, following the same strategy. As previously mentioned, for a single emitter being switched on, light data is only sensed by three to four receivers.

We explore another data-collection approach that dramatically increases the sampling rate. It involves concurrently switching on all the LEDs and continuously capturing the output image, requiring only one reading for all the emitters, thereby increasing the sampling rate by 24 (i.e. number of emitters). As illustrated in Figure 5a, this produces images with 24 circular dots, corresponding to the 24 optical fibres acting as receivers. Since the tips of all these optical fibres were spaced out from each others when fixed in front of the RGB camera, no overlapping light can be observed. Note that depending on the pressure being applied to the skin, the number and the intensity of the pixels corresponding to each receiver changes.

IV. Experiments

In this section, we compare the ability of our skin to estimate the location of an indenter pressing on the sensor skin as well as the amount of pressure being applied by a single contact. We acquire the sensor data concurrently and, for comparison, sequentially. Both estimation methods are

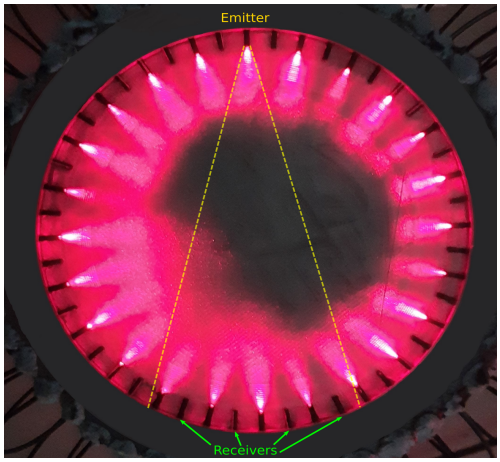

Fig. 4: Distribution of receiver and emitter optical fibres. The figure shows that light sent by an emitter will be captured by several receivers. The neighbouring receivers will be less illuminated than the optical fibre diametrically opposed to the emitter.

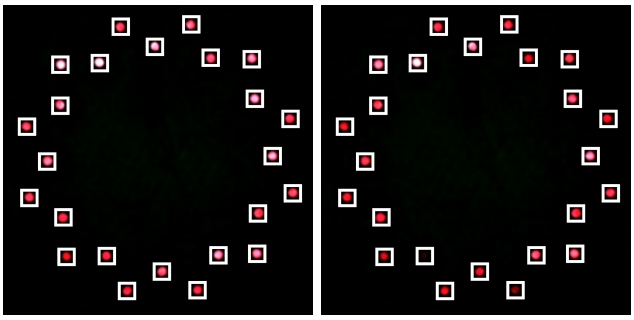

(a)

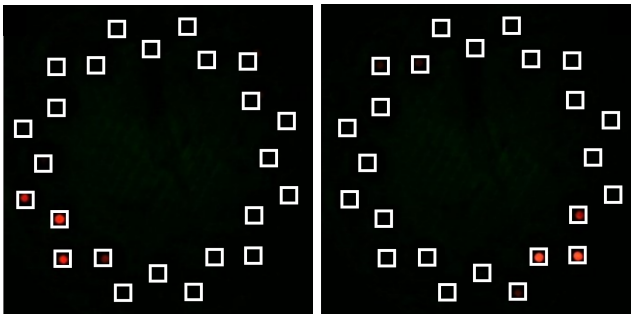

(b)

Fig. 5: Example of images collected during one reading of the sensor for both data collection strategy. (a) shows images captured when the skin is at rest (left) and pressed (right) for all LEDs concurrently switched on. (b) illustrates 2 of the 24 images collected during a reading when each emitter LED is switched on sequentially.

performed using Machine Learning models available in the `scikit-learn` library [23].

A. Data collection

The same protocol was used to collect data for both concurrent and sequential switching of the LEDs. A 5mm diameter flat ended indenter is mounted on an Universal Testing Machine (Instron 5967) to sequentially apply a set of 18 forces per node. The force applied by the Universal Testing machine is set to increase from 0.2 to 3N in increments of 0.2, but also to include $0.5, 1.5$ and 2.5N. For each condition (i.e. for each node and for each force), 30 readings are collected. In order for our model to be able to recognize when the skin is at rest (i.e. no force being applied), we also collect $30 \times 60 = 1800$ samples with no indention applied to the skin, for both concurrent as well as sequential methods.

B. Data processing

As illustrated in Figure 5, manually determined bounding boxes were used to estimate the light intensity sensed by all receiver fibres from each image captured by the camera. The 24 bounding boxes share the same size of 16×16 pixels. Each captured image follows the same processing steps. Firstly, the image is converted to grey-scale. Secondly, the mean value of each optical fibre bounding box is computed. By concatenating these 24 values, we obtain a feature vector describing the sensor image.
For the concurrent lighting approach, each reading is thus compressed into a vector containing 24 values representing the light intensity of each optical fibre. It is important to note that the 16×16 area accounts for the variation of number of illuminated pixels that can appear when the skin is pressed, making sure we retain all the light data captured by the camera. For the second lighting approach (sequential), vectors extracted from each image part of the reading are concatenated, leading to a feature vector containing $24 \times 24 = 576$ values. Regardless of the lighting condition, each feature vector is assigned with two labels; the index of the node on which the indenter is applied as well as the corresponding pressure.

C. Pressure localisation

By having artificially discretized the surface of our sensor into 60 nodes, we effectively reformulate the problem of localising the deformation of the skin into a classification problem. Inspired by the promising results reported in [21], we evaluate classical ML techniques to predict the index of the node being deformed by the indenter. As we want our classifier to be able to detect the localisation of the indentation regardless of the amount of pressure applied, we make use of the data collected for all the nodes, and for each of the 18 pressures considered during data collection. This leads to a total of $30 \times 18 = 540$ samples per node. In order to keep a balanced dataset, we also randomly extract the same number (540) of samples obtained when no pressure is applied to the skin, labeled as '0'. A third dataset is considered for training (keeping the same proportion of samples from each node and each pressure), totalling $10 \times 18 \times 61 = 10980$ samples while the remaining data is used to evaluate the generalisation of the model. A total of 3 classifiers (Random Forest [24], AdaBoost [25], SVM [26]) are trained to distinguish between the 61 classes (60 nodes + no pressure applied). We base our comparison on the accuracy and F1-score metrics, widely used in the literature to compare non-binary classification

tasks. While the accuracy corresponds to the proportion of correct predictions, the F1-score conveys the balance between the precision and the recall, i.e. the balance between sensitivity and specificity.

D. Pressure estimation

We formulate the task of estimating the pressure P applied to the soft skin as a regression problem. Since pressure localisation is achieved over the sensing area, we want this model to be able to estimate the pressure being applied anywhere on the sensor (i.e. on any node). The number of samples corresponding to each of the 18 pressures applied during data collection is hence $30 \times 60 = 1800$. We design the training set to contain 10 samples of each node for the $P \in \{0, 20.37, 30.56, 50.93, 71.30, 91.67, 112.04, 132.42, 152.79\}$ kPa, leading to a total of $10 \times 60 \times 9 = 5400$ feature vectors. The remaining samples for these particular pressures are used as validation set. Since we also want to evaluate our regression model on pressures never seen during training, we create a test set made of all the data corresponding to the other pressures. For this task, a set of 3 regressors (AdaBoost, Random Forest and SVM) are considered. Here, we base our comparison on the Root Mean Squared Error (RMSE) between the ground truth and the predicted values over a given data set. The lower the RMSE, the more accurate the estimation of the pressure being applied.

V. Results

A. Pressure localisation

For each data collection strategy, the accuracy and F1-score of the three classifiers used to predict the index of the node on which pressure as been applied are reported in Table I. Note that the reported results correspond to the performance of the classifiers when tested with all the pressures considered in this experiment.

TABLE I: Accuracy and F1-score comparison for node localisation between sequential and concurrent switching of LEDs for 3 classifiers

	AdaBoost		Random Forest		SVM	
	Acc.	F1	Acc.	F1	Acc.	F1
Sequential	0.542	0.555	**0.703**	0.697	0.699	**0.706**
Concurrent	0.656	0.669	0.903	0.898	**0.911**	**0.907**

Interestingly, the reported metrics are consistently higher, regardless of the classifier, when data is collected via our approach, when LEDs are switched concurrently. Overall, the best classifier is the SVM that achieves an accuracy of 91.1% and a F1-score of 90.7% when run on the data collected concurrently. For this classifier, we can observe that using concurrent switching of all the LEDs leads to an increase of more than 20 points in both accuracy and F1-score. A further analysis of the performance (not detailed here due to space constraint) show that most of the mis-classifications correspond to the SVM predicting a node in the direct neighbourhood of the ground truth. By virtue of the design of the virtual grid, the maximum localisation error is hence in the order of 7.5mm. The best classification model considered in this work runs in 29 ms, which means that for each image collected by the sensor, the model is capable to predict the localisation of the force applied without introducing any delay (value obtained on i5-4200U CPU @ 1.60GHz 2.30 GHz with 16GB RAM).

B. Pressure estimation

For each data collection approach and for each regressor the final RMSE obtained on the validation and test sets is reported in Table II.

TABLE II: Validation and test RMSE comparison for pressure estimation between sequential and concurrent switching of LEDs for 3 regressors

	AdaBoost		Random Forest		SVM	
	Valid	Test	Valid	Test	Valid	Test
Sequential	35.2	35.7	**24.1**	**30.9**	37	36.4
Concurrent	32.4	32.6	**14.5**	**17.2**	26.6	27.7

As with pressure localisation, the estimation of the pressure deforming the skin is consistently better for data collected concurrently, regardless of the ML method. For this task, it seems that Random Forest is the most suitable regressor, as it estimates the applied pressure with the lowest error, even for pressure values not considered during training. For concurrent switching of the LEDs, the RMSE values of the three regressors for different pressures are reported in Figure 6. The best regressor (i.e. Random Forest) demonstrates a similar performance as the one reported in [21] for $P \in [50.93, 152.79]$ kPa. However, the regressor is not capable of accurately estimating pressures within the range $]0, 50.93[$ kPa, as it reports a larger RMSE (e.g 17.84 for 25.46 kPa). In practice, our optical skin is therefore capable of recognizing that a pressure below 50.93 kPa is applied and can estimate with a good degree of accuracy the value of any pressure above or equal to 50.93 kPa. The best regression model considered in this work runs in 24 ms, which means that for each image collected by the sensor, the model is capable to estimate the amount of force being applied without introducing any delay.

VI. Conclusions

In contrast to standard tomography where lights are switched on sequentially, we propose in this paper a novel approach in which all light sources are switched on concurrently. The results of our experiments show that this approach not only dramatically increases the sample rate (by at least 24-fold), but also improves both pressure localisation and pressure estimation performance. We report an accuracy of 91.1% when trying to localise where the skin is indented, even for small indentation pressures, with a maximum error of 7.5 mm. For pressure localisation performance, the concurrent approach outperforms the sequential one by more than 20 points. We also demonstrate that our approach allows for a robust estimation of applied pressures of 50.93 kPa or above. Since the sensor only consists of soft and deformable materials, we intend to deploy this sensing technology in soft robots to improve their exteroceptive capabilities. In the

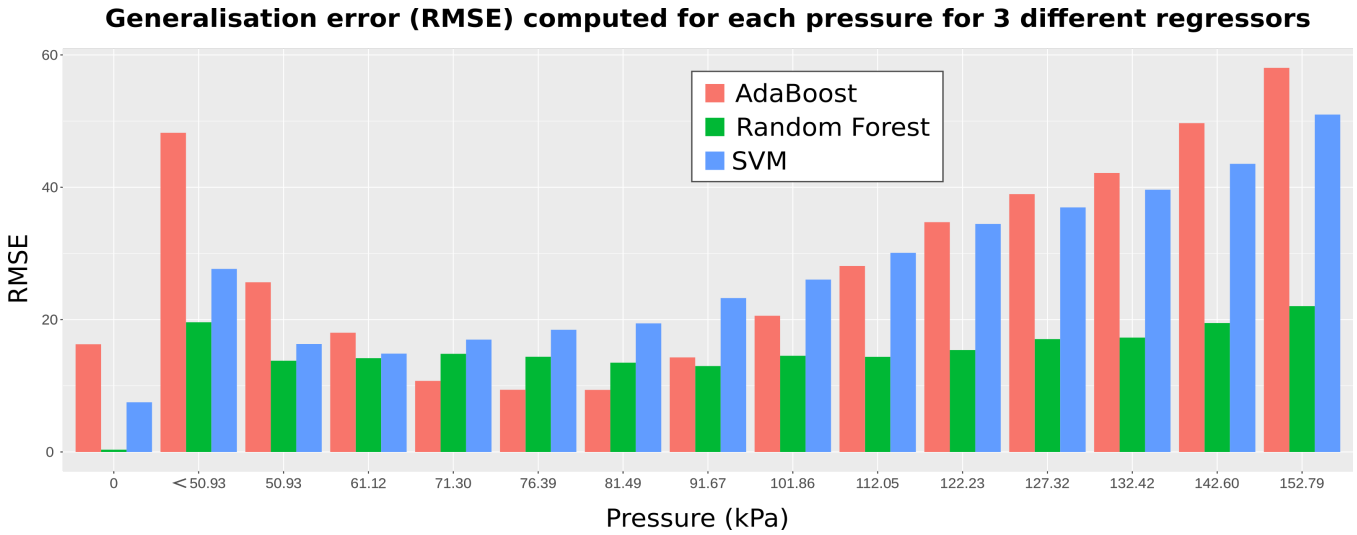

Fig. 6: Generalisation error (RMSE) of each regressor for different values of applied pressure with concurrent switching of the LEDs. These values are obtained on samples belonging to the validation and test set (i.e. not used for training).

future, we plan to further increase the pressure estimation and localisation performance by employing Deep Learning techniques - specifically Convolutional Neural Networks as they are principally designed to work with images. In order to extend the predictions of the Machine Learning model to further use-cases, we also plan to collect a novel dataset consisting of multiple and simultaneous contacts of the skin.

References

[1] C. Lee, M. Kim, Y. J. Kim, N. Hong, S. Ryu, H. J. Kim, and S. Kim, "Soft robot review," *International Journal of Control, Automation and Systems*, vol. 15, no. 1, pp. 3–15, 2017.

[2] F. Schmitt, O. Piccin, L. Barbé, and B. Bayle, "Soft robots manufacturing: A review," *Frontiers in Robotics and AI*, vol. 5, p. 84, 2018.

[3] J. Fras and K. Althoefer, "Soft biomimetic prosthetic hand: Design, manufacturing and preliminary examination," in *2018 IEEE/RSJ International Conference on Intelligent Robots and Systems (IROS)*. IEEE, 2018, pp. 1–6.

[4] A. B. Dawood, J. Fras, F. Aljaber, Y. Mintz, A. Arezzo, H. Godaba, and K. Althoefer, "Fusing dexterity and perception for soft robot-assisted minimally invasive surgery: What we learnt from stiff-flop," *Applied Sciences*, vol. 11, no. 14, p. 6586, 2021.

[5] D. Rus and M. T. Tolley, "Design, fabrication and control of soft robots," *Nature*, vol. 521, no. 7553, pp. 467–475, 2015.

[6] J. Tapia, E. Knoop, M. Mutnỳ, M. A. Otaduy, and M. Bächer, "Makesense: Automated sensor design for proprioceptive soft robots," *Soft robotics*, vol. 7, no. 3, pp. 332–345, 2020.

[7] M. Totaro, A. Mondini, A. Bellacicca, P. Milani, and L. Beccai, "Integrated simultaneous detection of tactile and bending cues for soft robotics," *Soft robotics*, vol. 4, no. 4, pp. 400–410, 2017.

[8] H. Wang, M. Totaro, and L. Beccai, "Toward perceptive soft robots: Progress and challenges," *Advanced Science*, vol. 5, no. 9, p. 1800541, 2018.

[9] S. Cheng, Y. S. Narang, C. Yang, Z. Suo, and R. D. Howe, "Stick-on large-strain sensors for soft robots," *Advanced Materials Interfaces*, vol. 6, no. 20, p. 1900985, 2019.

[10] A. B. Dawood, H. Godaba, A. Ataka, and K. Althoefer, "Silicone-based capacitive e-skin for exteroception and proprioception," in *2020 IEEE/RSJ International Conference on Intelligent Robots and Systems (IROS)*. IEEE, 2020, pp. 8951–8956.

[11] A. Dwivedi, A. Ramakrishnan, A. Reddy, K. Patel, S. Ozel, and C. D. Onal, "Design, modeling, and validation of a soft magnetic 3-d force sensor," *IEEE Sensors Journal*, vol. 18, no. 9, pp. 3852–3863, 2018.

[12] H. Cho, H. Lee, Y. Kim, and J. Kim, "Design of an optical soft sensor for measuring fingertip force and contact recognition," *International Journal of Control, Automation and Systems*, vol. 15, no. 1, pp. 16–24, 2017.

[13] T. G. Thuruthel, B. Shih, C. Laschi, and M. T. Tolley, "Soft robot perception using embedded soft sensors and recurrent neural networks," *Science Robotics*, vol. 4, no. 26, 2019.

[14] D. M. Vogt, Y.-L. Park, and R. J. Wood, "Design and characterization of a soft multi-axis force sensor using embedded microfluidic channels," *IEEE sensors Journal*, vol. 13, no. 10, pp. 4056–4064, 2013.

[15] C. Larson, B. Peele, S. Li, S. Robinson, M. Totaro, L. Beccai, B. Mazzolai, and R. Shepherd, "Highly stretchable electroluminescent skin for optical signaling and tactile sensing," *Science*, vol. 351, no. 6277, pp. 1071–1074, 2016.

[16] R. Dahiya, N. Yogeswaran, F. Liu, L. Manjakkal, E. Burdet, V. Hayward, and H. Jörntell, "Large-area soft e-skin: The challenges beyond sensor designs," *Proceedings of the IEEE*, vol. 107, no. 10, pp. 2016–2033, 2019.

[17] P. Maiolino, M. Maggiali, G. Cannata, G. Metta, and L. Natale, "A flexible and robust large scale capacitive tactile system for robots," *IEEE Sensors Journal*, vol. 13, no. 10, pp. 3910–3917, 2013.

[18] W. Yuan, S. Dong, and E. H. Adelson, "Gelsight: High-resolution robot tactile sensors for estimating geometry and force," *Sensors*, vol. 17, no. 12, p. 2762, 2017.

[19] L. Van Duong and V. A. Ho, "Large-scale vision-based tactile sensing for robot links: Design, modeling, and evaluation," *IEEE Transactions on Robotics*, vol. 37, no. 2, 2021.

[20] W. Li, Y. Noh, A. Alomainy, I. Vitanov, Y. Zheng, P. Qi, and K. Althoefer, "F-touch sensor for three-axis forces measurement and geometry observation," in *2020 IEEE Sensors*. IEEE, 2020, pp. 1–4.

[21] D. O. Amoateng, M. Totaro, M. Crepaldi, E. Falotico, and L. Beccai, "Intelligent position, pressure and depth sensing in a soft optical waveguide skin," in *2019 2nd IEEE International Conference on Soft Robotics (RoboSoft)*. IEEE, 2019, pp. 349–354.

[22] J. Gunther and S. Andersson-Engels, "Review of current methods of acousto-optical tomography for biomedical applications," *Frontiers of Optoelectronics*, vol. 10, no. 3, pp. 211–238, 2017.

[23] L. Buitinck, G. Louppe, M. Blondel, F. Pedregosa, A. Mueller, O. Grisel, V. Niculae, P. Prettenhofer, A. Gramfort, J. Grobler, R. Layton, J. VanderPlas, A. Joly, B. Holt, and G. Varoquaux, "API design for machine learning software: experiences from the scikit-learn project," in *ECML PKDD Workshop: Languages for Data Mining and Machine Learning*, 2013, pp. 108–122.

[24] T. K. Ho, "Random decision forests," in *Proceedings of 3rd international conference on document analysis and recognition*, vol. 1. IEEE, 1995, pp. 278–282.

[25] R. E. Schapire, "Explaining adaboost," in *Empirical inference*. Springer, 2013, pp. 37–52.

[26] C. Cortes and V. Vapnik, "Support-vector networks," *Machine learning*, vol. 20, no. 3, pp. 273–297, 1995.